Non-Markovian approach to globally coupled excitable systems

T. Prager,[1] M. Falcke,[2] L. Schimansky-Geier,[1] and M. A. Zaks[1]
[1]*Institute of Physics, Humboldt-University of Berlin, Newtonstrasse15, 12489 Berlin, Germany*
[2]*Department of Theory, Hahn-Meitner-Institute, Glienicker Strasse 100, 14109 Berlin, Germany*
(Received 6 March 2007; published 24 July 2007)

We consider stochastic excitable units with three discrete states. Each state is characterized by a waiting time density function. This approach allows for a non-Markovian description of the dynamics of separate excitable units and of ensembles of such units. We discuss the emergence of oscillations in a globally coupled ensemble with excitatory coupling. In the limit of a large ensemble we derive the non-Markovian mean-field equations: nonlinear integral equations for the populations of the three states. We analyze the stability of their steady solutions. Collective oscillations are shown to persist in a large parameter region beyond supercritical and subcritical Hopf bifurcations. We compare the results with simulations of discrete units as well as of coupled FitzHugh-Nagumo systems.

DOI: 10.1103/PhysRevE.76.011118 PACS number(s): 05.40.−a, 05.45.Xt, 05.10.Gg, 84.35.+i

I. INTRODUCTION

Waiting time density functions are an efficient tool for a description of complex stochastic processes [1,2]. They have been successfully applied in studies of random walks [5], spin glasses [3], self-organized criticality [4], reaction-transport systems [6], turbulence [7], quenched disorder [8], fractals [9], and in many other contexts. We will apply them here to develop a theory of hierarchical stochastic systems.

The general scheme in which the notion of a waiting time density function becomes useful is a multistate process, in the course of which a small subset of events drives the dynamics on a higher level of structure. As an example, consider an ion channel of a neuron. Its opening and closing controls the currents which determine the membrane voltage dynamics of the cell. Each individual act of opening and closing is the outcome of a complex interaction of many channel subunits. This interaction may involve many different open and closed states of the channel. However, only the opening and closing events are relevant for the membrane potential. Consequently, a description of the membrane potential dynamics can be based on waiting time density functions for transitions to and from the closed and open states, respectively.

Such a description can reduce the multistate master equation governing the complete system to a low-dimensional set of evolution equations for the probability density function. The price to pay for hiding the complex-state dynamics in the waiting time density functions is a non-Markovian formulation of the problem [10]. Here, we aim to demonstrate that waiting time densities and the evolution equations are efficient tools for describing the collective behavior on a certain structural level without losing information on the stochastic behavior of the underlying level.

Our studies are directed at phenomena in coupled excitable dynamics [11,12]. Many types of ion channels can be viewed as realizations of a stochastic excitable system [13,14]. These excitable systems can be mapped onto alternating transitions between three discrete states: a rest state, an excited (or firing) state, and an inhibited state, often also called a refractory state [15].

The excitation loop involves transitions from the rest state to the excited state, from there to the refractory state and finally back to the rest state. The first transition requires one to overcome a threshold below which the system relaxes back to the rest state. This threshold may be surpassed due to spontaneous fluctuations or due to an external excitation. Supplementing the discrete-state scheme by waiting time density functions completes the characterization of the excitable unit. In general, waiting time density functions describe non-Markovian transition rules [10].

Excitable systems under the influence of noise turned out to be especially capable of generating spatial and temporal structures. Indeed, connected networks of coupled stochastic elements are among the main topics in current complex systems research [16–19]. They can be observed in a variety of different physical, chemical, biological, and sociological frameworks [2,14,20–32].

A specific type of collective behavior of stochastic excitable media is the excitation of global oscillations accompanied by mutual synchronization of the individual units [16,17,33–36]. It is due to the amplification of an oscillatory mode which occurs at moderate noise intensity [37–40]. Known under the name of coherence resonance [12,41], this phenomenon is reflected by an increase of the correlation time under the growth of noise. When coupled, such units exhibit collective oscillations.

Many analytical and numerical studies have investigated stochastic excitable models as Markovian ones with a variety of methods: e.g., using continuous phase variables, leaky integrate-and-fire-models, and two-variable systems (see [2,12,23,28,29] for a review). Here, we introduce a simple non-Markovian three-state model of an excitable system [11] which is represented by a semi-Markov process [10,42] for a single unit. We construct a renewal process with three discrete states. Waiting time density functions in the excited and refractory states are nonexponential functions, but the transitions do not possess memory: Time spent in a certain state is independent of the time spent in the preceding state.

In the current paper, the excitable unit is given by a noisy FitzHugh-Nagumo (FHN) system in the excitable regime. The FHN system is known to mimic the action of a simple neuron gated by ion channels [43]. To infer the waiting time

density from dynamics is a highly nontrivial task [2,44–48]. Therefore we decided to model the waiting times in the discrete states by Γ-density functions; parameters of the latter are adjusted to match FitzHugh-Nagumo dynamics.

A detailed description as well as a discussion of the dynamical properties of the excitable unit is given in the following section. Subsequent sections are devoted to coupled ensembles. First, we outline a mean-field theory for the occupation numbers of the three states in the globally coupled ensemble and derive a system of integro-differential equations for their dynamics.

In general, such equations operate in infinite-dimensional spaces. However, for certain "resonant" density functions of the waiting times in which the ratios of higher moments to the mean values are integers, non-Markovian dynamics can be reduced to a finite number of ordinary differential equations. That provides the basis for bifurcation analysis. In this case a full treatment of the stability for steady solutions of the mean-field equation is possible.

We demonstrate for a paradigmatic type of coupling that the onset of oscillations occurs via the Hopf bifurcation. Depending on the parameters, the bifurcation can be either supercritical or subcritical; this matches the results of numeric simulations of coupled continuous FHN units. Special emphasis in the discussion is given to the role of the non-Markovian character of transition rules, to the role of noise, and to effects which are due to coupling.

II. THREE-STATE MODEL OF AN EXCITABLE STOCHASTIC SYSTEM

A. Waiting time densities of excitable systems

Excitability is characterized by the response of a dynamical system to external perturbations. If the perturbations are small, the system remains close to its stable time-independent state, which we call the rest state. In the case of large perturbations exceeding a certain threshold the system switches to the excited state where it performs a long excursion in phase space before it goes to the refractory state. There it remains a certain time and is insensitive to perturbations before it returns to the initial state.

A typical excitable system which demonstrates this behavior is the FitzHugh-Nagumo model. Its two-dimensional dynamics in the presence of noise is governed by

$$\dot{x} = x - x^3 - y + f(t) + \sqrt{2D}\xi(t),$$

$$\dot{y} = \varepsilon(x + a_0 - a_1 y). \tag{1}$$

Here, the variable $x(t)$ stands for the activator corresponding to the membrane voltage in neuron models, whereas $y(t)$ describes the inhibitor or the recovery variable. Further, ε is the parameter of the time-scale separation between activator and inhibitor, and a_0 and a_1 characterize, respectively, the value of the threshold and the decay time of the inhibitor. In the first equation, $f(t)$ denotes an external input and $\xi(t)$ is the δ-correlated Gaussian white noise with intensity D and zero mean.

The nullclines in case of vanishing noise and two fixed inputs $f_{1/2}$ are shown in Fig. 1 together with a typical stochastic trajectory. We see that the inputs yield a shift of the relative position of the nullclines and might induce a bifurcation from excitable to oscillatory behavior. In a coarse-grained description, we will distinguish between states with $(x<0)$ corresponding to the gray-shaded region in Fig. 1 and states with $(x>0)$ colored in light gray. Both states contain the two attracting branches of the nullcline $\dot{x}=0$ and are connected by fast transitions in the limit of small ε.

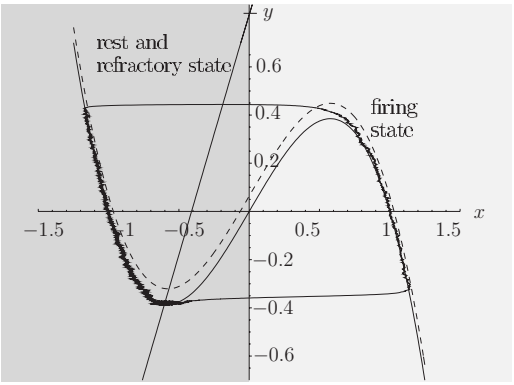

FIG. 1. Nullclines $\dot{x}=0$ and $\dot{y}=0$ for the FHN model: Eq. (1) with $a_0=0.41$, $a_1=0.5$, and $D=0$. Two variants of the fixed external input f are shown: $f=0$ (solid line) and $f=0.01$ (dashed line). A typical trajectory which runs along the attracting branches and switches between them is plotted for $\varepsilon=0.01$, $f=0$, and $D=10^{-4}$.

We have simulated two waiting time densities of these two states. The top panel in Fig. 2 shows waiting time densities $w_{x<0}(\tau)$ for staying in the state $x<0$, whereas the bottom panel presents the waiting time density $w_{x>0}(\tau)$ of the excited or firing state $x>0$, respectively. The curves in both figures are not normalized. The times in the excited state $x>0$ are rather unaffected by the change of noise and of the input values. Also the time lag of the upper curve is nearly independent of the parameters whereas the exponential decay at longer times depends strongly if varying the input f.

One can easily realize that the behavior in the region with $x<0$ corresponds to a convolution of two sequential events:

$$w_{x<0}(\tau) = \int_0^\tau d\tau'\ w_{\mathrm{ref}}(\tau') w_{\mathrm{rest}}(\tau - \tau'). \tag{2}$$

A nearly fixed waiting time up to $\tau=200$ is followed by a second step which is well approximated by an exponential waiting time density. Thus we will introduce in our model two discrete states for the temporal evolution at the left stable branch. First, trajectories spend a time distributed by $w_{\mathrm{ref}}(\tau)$, a refractory state. It corresponds to the time of motion along the left stable branch of the cubic nullcline in order to relax to the stable fixed point. Qualitatively the refractory times behave similar to the firing times; i.e., $w_{\mathrm{ref}}(\tau)$ would take a shape like the curves of $w_{x>0}$ in the bottom panel of Fig. 2 but centered around $\tau\approx 200$ for the selected parameters.

The relaxation is followed by the rest state, where the system stays a time distributed by $w_{\mathrm{rest}}(\tau)$. This rest state corresponds to the fixed point of the FHN system and es-

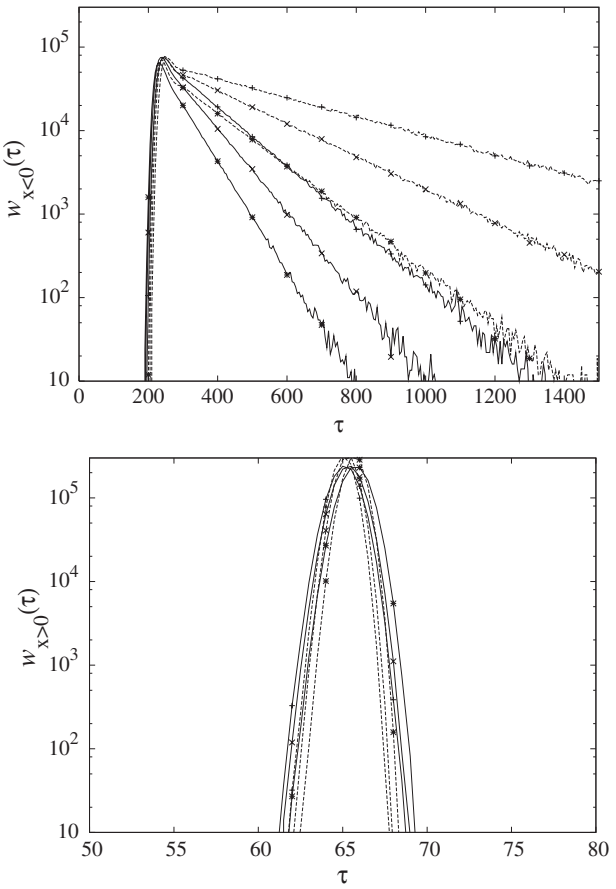

FIG. 2. Waiting time density functions (not normalized) in states with $x<0$ (top) and with $x>0$ (bottom) in logarithmic scale for a FHN system with $a_0=0.41$, $a_1=0.5$, and $\varepsilon=0.01$ for two values of the noise strength: $D=0.0001$ (gray) and $D=0.0002$ (black). Different symbols represent different constant values of the external signal $f_{1,2,3}$. $\star$: $f_1=-0.01$. $\times$: $f_2=0.0$. Bottom: $+$: $f_3=0.01$.

capes to the firing branch, which occurs as a noise-assisted activation process with a constant rate. Therefore, in accordance with results in Fig 2 we assume an exponentially distributed waiting time in this state. The rate depends on the magnitude of the external input f which corresponds to the different decays in the top panel of Fig. 2.

Thus, summarizing, these dynamical features can be modeled by a discrete non-Markovian three-state system (see Fig. 3) with states $\sigma=1,2,3$ and waiting time densities $w_1(t)$, $w_2(t)$, and $w_3(t)$ to stay time t therein. The rest state [further on it will be labeled by $\sigma=1$ and $w_1(t)=w_{\text{rest}}(t)$] corresponds to the dynamics near the stable fixed point. The system escapes from the fixed point to the excited state by a rate process with constant rate γ. The probability of excitation in Δt has no memory and is independent of the time already spent in this state. It is thus given by

$$w_1(t) = \gamma \exp(-\gamma t), \tag{3}$$

where both the mean and the standard deviation equal $1/\gamma$.

Two additional states $\sigma=2$ and $\sigma=3$ correspond to the excited and refractory states with $w_2(t)=w_{x>0}(t)$ and $w_3(t)$

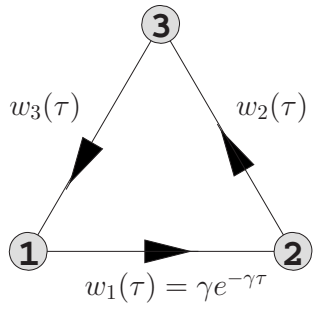

FIG. 3. Three-state model of an excitable unit. State 1 assigns the rest state, followed by the excited (firing) state 2. State 3 stands for the refractory state. The process $1\to2$ is a Markovian rate process, while the transitions $2\to3$ and $3\to1$ are characterized through waiting time density functions $w_2(\tau)$ and $w_3(\tau)$, respectively.

$=w_{\text{ref}}(t)$. At low noise levels, the excited state 2 and refractory state 3 are left after approximately constant waiting times τ_2 and τ_3, respectively. If we neglect fluctuations, the waiting time densities become δ functions:

$$w_2(t) = \delta(t-\tau_2),$$

$$w_3(t) = \delta(t-\tau_3). \tag{4}$$

Upon increasing the noise level, the variance of these density functions grows as well. We model this behavior by a Γ-density function

$$w_2(\tau) = \frac{\alpha_2}{\tau_2\Gamma(\alpha_2)}\left(\frac{\alpha_2 t}{\tau_2}\right)^{\alpha_2-1}\exp\left(-\frac{\alpha_2 t}{\tau_2}\right), \tag{5a}$$

$$w_3(\tau) = \frac{\alpha_3}{\tau_3\Gamma(\alpha_3)}\left(\frac{\alpha_3 t}{\tau_3}\right)^{\alpha_3-1}\exp\left(-\frac{\alpha_3 t}{\tau_3}\right). \tag{5b}$$

The parameters α_2 and α_3 serve as a measure of the sharpness of the transitions $2\to3$ and $3\to1$, respectively. For $\alpha_{2,3}=1$ the waiting times are exponentially distributed and the variance equals the mean value. In contrast, at $\alpha_{2,3}\to\infty$ the variances vanish: we obtain δ-distributed waiting times. In case of integer α_i the Γ-density functions are known under the name of Erlang distributions. Mean values and variances of waiting times distributed according to Eqs. (5a) and (5b) are given by ($\sigma=2,3$)

$$\langle\tau\rangle_\sigma := \int_0^\infty d\tau\, \tau w_\sigma(\tau) \equiv \tau_\sigma$$

and

$$\langle\Delta\tau^2\rangle_\sigma := \int_0^\infty d\tau\, \tau^2 w_\sigma(\tau) - \langle\tau\rangle_\sigma^2 = \frac{\tau_\sigma^2}{\alpha_\sigma}.$$

The shapes of the Γ-density functions for three different variances are plotted in Fig. 4.

B. Non-Markovian dynamics of excitability

The following balance equations hold for the probabilities $P_\sigma(t)$, $\sigma=1,2,3$, to be in state σ at time t:

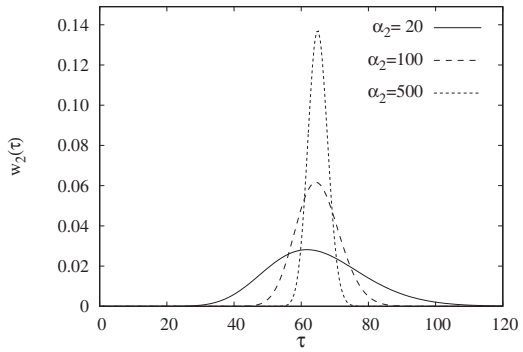

FIG. 4. Γ-density function [Eq. (5a) and (5b)] versus waiting time τ_2 with $\langle\tau\rangle=65$, for different values of α_2.

$$\frac{d}{dt}P_1(t) = -J_{1\to2}(t) + J_{3\to1}(t), \tag{6a}$$

$$\frac{d}{dt}P_2(t) = -J_{2\to3}(t) + J_{1\to2}(t), \tag{6b}$$

$$\frac{d}{dt}P_3(t) = -J_{3\to1}(t) + J_{2\to3}(t), \tag{6c}$$

where $J_{\sigma\to\bar{\sigma}}(t)$ denotes the probability flux from state σ to state $\bar{\sigma}$ at time t. Since the transition from state 1 to 2 is a rate process, the probability flux $J_{1\to2}(t)$ can be expressed in terms of the probability to be in state 1 as

$$J_{1\to2}(t) = \gamma P_1(t).$$

Let us assume that the system has started in state 1 at time t_0. Then the probability flux $J_{2\to3}(t)$ from state 2 to 3 at time t is expressed by the product of the probability flux from state 1 to 2 at an earlier time t' between t_0 and t with the probability density w_2 to wait in state 2 from t' until t:

$$J_{2\to3}(t) = \int_{t_0}^{t} dt'\ J_{1\to2}(t')w_2(t-t').$$

In the same way, the flux from state 3 to 1 is

$$J_{3\to1}(t) = \int_{t_0}^{t} dt'\ J_{1\to2}(t')(w_2 \circ w_3)(t-t').$$

where the convolution is defined as $(w_2 \circ w_3)(\tau) = \int_0^\tau d\tau'\ w_2(\tau')w_3(\tau-\tau')$. Taken together, Eqs. (6a)–(6c) read

$$\frac{d}{dt}P_1(t) = -\gamma P_1(t) + \int_{t_0}^{t} dt'\ J_{1\to2}(t')(w_2 \circ w_3)(t-t'), \tag{7a}$$

$$\frac{d}{dt}P_2(t) = -\int_{t_0}^{t} dt'\ J_{1\to2}(t')w_2(t-t') + \gamma P_1(t), \tag{7b}$$

$$\frac{d}{dt}P_3(t) = -\int_{t_0}^{t} dt'\ J_{1\to2}(t')(w_2 \circ w_3)(t-t') + \int_{t_0}^{t} dt'\ J_{1\to2}(t')w_2(t-t'). \tag{7c}$$

These equations are supplemented by the initial condition $P_\sigma(t_0)=\delta_{\sigma,1}$.

Integrating Eqs. (7a)–(7c) with respect to t, taking into account the initial condition, and passing to the asymptotic limit $t_0\to-\infty$ finally leads to the set of integral equations for the asymptotic probabilities

$$P_2(t) = \int_0^\infty d\tau\ \gamma P_1(t-\tau)z_2(\tau),$$

$$P_3(t) = \int_0^\infty d\tau \int_0^\infty d\tau'\ \gamma P_1(t-\tau-\tau')w_2(\tau)z_3(\tau'),$$

$$P_1(t) = 1 - P_2(t) - P_3(t). \tag{8}$$

Here

$$z_\sigma(\tau) = \int_\tau^\infty d\tau'\ w_\sigma(\tau') \tag{9}$$

denotes, respectively, the probabilities to survive longer than τ in states $\sigma=2,3$.

C. Spectral properties

To demonstrate that the dynamics of each individual unit shows typical features of excitable systems we inspect its power spectrum. We set the output in correspondence to the activator of the FitzHugh-Nagumo system $s=1$ if the unit is in state $\sigma=2$ at time t and $s=-1$ otherwise. Then the spectrum is determined employing renewal theory [11,49]:

$$S(\omega) = \frac{4}{\left(T+\frac{1}{\gamma}\right)\omega^2}\frac{\sin^2\frac{\omega\tau_2}{2}}{1+2\frac{\gamma^2}{\omega^2}(1-\cos\,\omega T)+\frac{\gamma}{\omega}\sin\,\omega T}, \tag{10}$$

where $T=\tau_2+\tau_3$ and $\bar{w}=T+1/\gamma$. The stochasticity of the process can be controlled by varying the amount of time spent in state 1 compared to T. If $1/\gamma \gg T$, the system spends most of the time in state $\sigma=1$ and the stochasticity of the first step dominates the dynamics. In contrast, for $1/\gamma \ll T$ the process is similar to oscillations. We show the spectral power density of the three-state model with waiting time density functions, Eqs. (3), (5a), and (5b), and the power density of the output of the FHN model, Eqs. (1) in Fig. 5. The parameters of the waiting time density functions Eqs. (3), (5a), and (5b) were fit to match the spectrum of Eqs. (1).

III. ENSEMBLES OF COUPLED ELEMENTS

Now we will consider ensembles of N globally coupled three-state systems. The current state of the ensemble at time t is defined by the local variables $\sigma_i(t)=1,2,3$ with $i=1,\ldots,N$. As local output we again adopt the value $s_2=1$ to

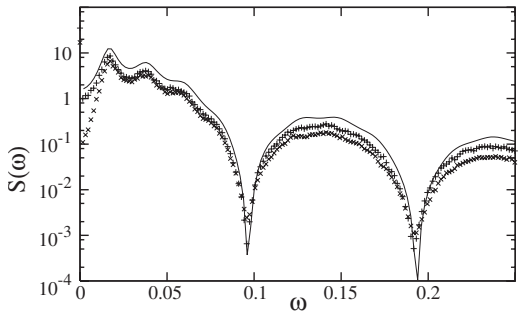

FIG. 5. Spectral power density given by Eq. (10) of a single three-state unit (solid line) with excitation rate $\gamma_0=0.0046$ and fixed waiting times $\tau_2=65$ and $\tau_3=220$ in states 2 and 3, respectively, compared to the spectral power density of the output $x(t)$ of the FitzHugh-Nagumo system, Eq. (1), with $a_0=0.41$, $a_1=0.5$, $\varepsilon=0.01$, $D=0.0001$, and $f(t)=0$ [× marks x(t), and + marks dichotomically filtered output 1 if $x(t)>0$ and −1 if $x(t)\leq 0$].

state 2 and we put $s_{2/3}=-1$ in the other two states. This choice is accordance with the behavior of a activator of a FitzHugh-Nagumo model.

In the previous section (Fig. 2) we found that weak signals acting on the FHN system essentially change the excitation rate γ while the motion along the excitation loop remains unaffected. Correspondingly, a prototypical global coupling between the individual excitable units is introduced by letting this rate depend on the value of the ensemble's global output $f(t)$:

$$f(t)=\frac{1}{N}\sum_{i=1}^{N} s_i(t). \tag{11}$$

Obviously $f(t)\varepsilon[-1,1]$. We express the global output $f(t)$ as the difference between the number of units in state 2 and the number of units in states 1 and 3 taken together—i.e., $N_2-(N_1+N_3)$. This expression can be rendered as

$$f(t)=\frac{n_2-(n_1+n_3)}{N}=2\frac{n_2(t)}{N}-1$$

in terms of the fraction $n_2(t)=N_2/N\ \varepsilon[0,1]$ of units in state 2. n_2 can be expressed as sum of units which are currently in the excited state and for which $\sigma_j=2$.

We thus consider in the following the rate γ to be dependent on $n_2(t)$ instead of $f(t)$. In detail, we assume as a prototypical model

$$\gamma=\gamma\left(\frac{1}{N}\sum_{i=1}^{N}\delta_{\sigma_i,2}\right)=\gamma\left(\frac{n_2}{N}\right)$$

to be the rate that the jth unit leaves its state $\sigma_j=1$. By definition the actual σ_j does not contribute to $n_2(t)$. In Sec. IV, γ will be specified as function of its argument. Schematically, the corresponding three-state unit is sketched in Fig. 6.

A. Derivation of mean-field equations

Let $p(\sigma_1,\ldots,\sigma_N,t)$ denote the probability that unit $i=1,\ldots,N$ is in state $\sigma_i=1,2,3$ at time t. The reduced probability $p_i^j(t)$ that unit j is in state i can be expressed by tracing out all the other units,

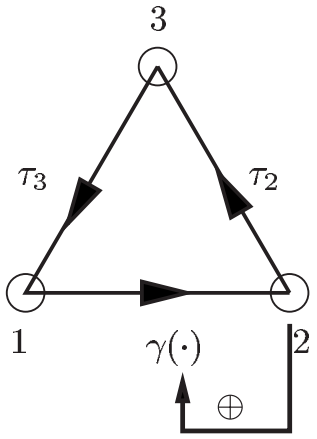

FIG. 6. Three-state model of an excitable unit. The process $1\to 2$ is Markovian, while the transitions $2\to 3$ and $3\to 1$ are deterministic with a fixed waiting time [Eqs. (4)] or obey Γ-density functions [Eqs. (5a) and (5b)]. The units are coupled by the dependence of γ on the ensemble output $f(t)$.

$$p_i^j(t):=\sum_{\{\sigma_j'\}=1}^{3} p(\sigma_1,\ldots,\sigma_{j-1},i,\sigma_{j+1},\ldots,\sigma_N,t). \tag{12}$$

We agree that $\{\sigma_j'\}$ denotes the complement of all possible states of the ensemble; i.e., it assigns a summation of $\sigma_k=1,2,3$ with k running over all units except j.

The governing equations for these single-unit probabilities can be derived in the same manner as Eq. (8); however, we have to take into account the dependence of the excitation rate γ on the state of all other units. With the help of definition (12) we obtain [50] for the probability that the jth unit is in state 2 by summation over $p(\sigma_1,\ldots,\sigma_{j-1},2,\sigma_{j+1},\ldots,\sigma_N,t)$, yielding

$$p_2^j(t)=\sum_{\{\sigma_j\}'=1}^{3}\int_0^\infty d\tau\,\gamma\left(\frac{1}{N}\sum_{i=1}^{N}\delta_{\sigma_i,2}\right)\times p(\sigma_1,\ldots,\sigma_{j-1},1,\sigma_{j+1},\ldots,\sigma_N,t-\tau)z_2(\tau). \tag{13a}$$

Respectively, for state 3, tracing out $p(\sigma_1,\ldots,\sigma_{j-1},3,\sigma_{j+1},\ldots,\sigma_N,t)$ leads to

$$p_3^j(t)=\sum_{\{\sigma_j\}'=1}^{3}\int_0^\infty d\tau\int_0^\infty d\tau'\,\gamma\left(\frac{1}{N}\sum_{i=1}^{N}\delta_{\sigma_i,2}\right)\times p(\sigma_1,\ldots,\sigma_{j-1},1,\sigma_{j+1},\ldots,\sigma_N,t-\tau-\tau')z_3(\tau)w_2(\tau'). \tag{13b}$$

On denoting by $p_N(n_1,n_2,n_3,t)$ the probability to find n_1 units in state 1, n_2 units in state 2, and n_3 units in state 3 we obtain the three relations, $i=1,2,3$,

$$\frac{1}{N}\sum_{j=1}^{N} p(i)^j(t) = \sum_{n_1,n_2,n_3=0}^{N} \frac{n_i}{N} p_N(n_1,n_2,n_3,t)\,\delta_{N,n_1+n_2+n_3}$$

and $\delta_{N,n_1+n_2+n_3}$ stands for the Kronecker symbol yielding a summation of all possibles triples with fixed overall N. Equations (13a) and (13b) can thus be rewritten as

$$\sum_{n_1,n_2,n_3=0}^{N} \delta_{N,n_1+n_2+n_3}\left[\frac{n_2}{N}p(n_1,n_2,n_3,t) - \frac{n_1}{N}\int_0^\infty d\tau\,\gamma\left(\frac{n_2}{N}\right)p(n_1,n_2,n_3,t-\tau)z_2(\tau)\right] = 0, \tag{14a}$$

$$\sum_{n_1,n_2,n_3=0}^{N} \delta_{N,n_1+n_2+n_3}\left[\frac{n_3}{N}p(n_1,n_2,n_3,t) - \frac{n_1}{N}\int_0^\infty d\tau\int_0^\infty d\tau'\,\gamma\left(\frac{n_2}{N}\right)p(n_1,n_2,n_3,t-\tau-\tau')z_3(\tau)w_2(\tau')\right] = 0. \tag{14b}$$

Next, we consider the limit of infinitely many coupled units $N\to\infty$ and neglect finite-size effects. The relative occupation numbers $n_i(t)/N$ converge to a deterministic process $P_i(t)$ in the following sense of weak convergence: We demand that the probability density function $p(n_1,n_2,n_3,t)$ become sharply peaked around the values $n_i=P_i(t)N$, such that an arbitrary continuous function f of the relative occupation numbers n_i/N obeys

$$\lim_{N\to\infty}\sum_{n_1,n_2,n_3=0}^{N}\delta_{N,n_1+n_2+n_3}p(n_1,n_2,n_3,t)f\left(\frac{n_1}{N},\frac{n_2}{N},\frac{n_3}{N}\right) = f(P_1(t),P_2(t),P_3(t)). \tag{15}$$

In this limit we then obtain from Eq. (14a)

$$P_2(t) = \int_0^\infty d\tau\,\gamma(P_2(t-\tau))P_1(t-\tau)z_2(\tau),$$

$$P_3(t) = \int_0^\infty d\tau\int_0^\infty d\tau'\,\gamma(P_2(t-\tau-\tau')) \times P_1(t-\tau-\tau')z_3(\tau)w_2(\tau'), \tag{16}$$

supplemented by the normalization condition

$$P_1(t) = 1 - P_2(t) - P_3(t).$$

Note that in the case of uncoupled systems in which the states of the units at all times t are independent random variables, the assumption (15) is just the law of large numbers.

B. Bifurcation analysis of the mean-field equations

The mean-field equations (16) constitute the starting point for the bifurcation analysis of the globally coupled system. In general, due to presence of the memory terms, these equations operate in infinite-dimensional space. Accordingly, in the stability analysis of different states, characteristic equations can possess an infinite number of roots. Analysis of those roots allows us to investigate possible bifurcations in the non-Markovian dynamics.

We begin with the calculation of steady states (fixed points in phase space). For this purpose, we substitute $P_k(t)=P_k^*$ in Eqs. (16) and use the obvious identity $\int_0^\infty d\tau\, z_i(\tau)=\int_0^\infty d\tau\,\tau w_i(\tau)=:\tau_i$. This leads to

$$P_2^* = \frac{\tau_2}{\tau_2+\tau_3+1/\gamma(P_2^*)},$$

$$P_3^* = \frac{\tau_3}{\tau_2}P_2^*, \tag{17}$$

and $P_1^*=1-P_2^*-P_3^*$. The stationary occupation probability of a state is the ratio between the mean time spent in this state and the mean time for one cycle. The mean waiting time in the rest state $1/\gamma(P_2^*)$ depends on the stationary occupation probability of state 2, rendering Eq. (17) implicit and, in general, nonlinear.

A remarkable property of Eq. (17) is the *absence* of the variances $\alpha_{2,3}$ of the waiting time density functions. Accordingly, the number of stationary states depends only on the mean waiting times $\tau_{2,3}$ and the function $\gamma(P)$. Consequently, the number of fixed points does not depend on $\alpha_{2,3}$.

To a certain extent, the analysis of stability does not require the explicit form of the function $\gamma(P)$; relevant are only the value of this function and its derivative γ' in the fixed point. It is convenient to interpret the results in terms of two "parameters" $r=\gamma(P_2^*)$ and $s=P_1^*\gamma'(P_2^*)$ [51].

To investigate the local stability of steady states, we add small perturbations $P_k(t)=P_k^*+c_k\exp(\lambda t)$ with $\Sigma_{k=1}^3 c_k\exp(\lambda t)=0$. Linearization of Eqs. (16) near the fixed point produces the characteristic equation

$$1+\frac{1}{\lambda}\{s[\hat{w}_2(\lambda)-1]+r[1-\hat{w}_2(\lambda)\hat{w}_3(\lambda)]\}=0, \tag{18}$$

where the Laplace transforms $\hat{w}_i(\lambda)=\int_0^\infty d\tau\, e^{-\lambda\tau}w_i(\tau)$ for the waiting times in the excited ($i=2$) and refractory ($i=3$) states given by Eqs. (5a) and (5b) are

$$\hat{w}_i(\lambda) = \left(1+\frac{\tau_i\lambda}{\alpha_i}\right)^{-\alpha_i}. \tag{19}$$

Depending on the waiting time density functions, the characteristic equation possesses several or even infinitely many complex roots.

We start with an ensemble of uncoupled units. In this case $\gamma(P)$ is constant, hence $s=0$; and Eq. (17) is explicit and has a unique solution. It can be shown that this solution is stable. Let us move in parameter space by gradually changing the dependence $\gamma(P)$ (and, possibly, the parameters τ_i and α_i as well).

On reaching for the first time the boundary

$$s = \frac{r(\tau_2 + \tau_3) + 1}{\tau_2}, \tag{20}$$

one of the real eigenvalues of the characteristic equation vanishes. This event corresponds to a saddle-node bifurcation of fixed points. As already mentioned, this bifurcation is independent of the variances $\alpha_{2,3}$. In general, new fixed points appear at some finite distance from the original fixed point and do not have an immediate effect on its stability. In the course of further changes of parameters, the "original" fixed point approaches one of the newborn fixed points, merges with it, and disappears in another saddle-node bifurcation.

If, additionally to Eq. (20), the second derivative

$$\frac{d^2}{dP^2}\left(\frac{\tau_2}{\tau_2 + \tau_3 + 1/\gamma(P)}\right)$$

vanishes at $P = P_2^*$, two separate folds merge in a pitchfork bifurcation. Explicitly, additional provision for this codimension-2 event reads as

$$\gamma''(P_2^*) = \frac{2(\tau_2 + \tau_3)\gamma'^2(P_2^*)}{1 + (\tau_2 + \tau_3)\gamma(P_2^*)}. \tag{21}$$

On a parameter route through the cusp point, two new steady states are born from the already existing one.

Typically, the second saddle-node bifurcation is preceded by the Hopf bifurcation: the original equilibrium acquires a pair of complex eigenvalues with positive real part. In contrast to the saddle node, the location of the Hopf bifurcation in the parameter space depends on $\alpha_{2,3}$. We are unable to formulate this bifurcation condition as a single expression which interrelates the critical values of r and s. Instead, we present it in parametric form where the parameter ω is the frequency of the critical marginal oscillations at the bifurcation point:

$$r_{\mathrm{Hopf}}(\omega) = \omega \frac{I_{23}(I_3 - I_{23}) + R_{23}(R_3 - R_{23})}{I_{23} - I_{23}R_3 - I_3 + I_3 R_{23}},$$

$$s_{\mathrm{Hopf}}(\omega) = -\omega \frac{I_{23}^2 + R_{23}(R_{23} - 1)}{I_{23} - I_{23}R_3 - I_3 + I_3 R_{23}}. \tag{22}$$

Here R_3 and I_3 denote, respectively, the real and imaginary parts of $(1 + i\omega\tau_3/\alpha_3)^{\alpha_3}$ whereas the abbreviations R_{23} and I_{23} stand, respectively, for the real and imaginary parts of the product $(1 + i\omega\tau_2/\alpha_2)^{\alpha_2}(1 + i\omega\tau_3/\alpha_3)^{\alpha_3}$. Of course, only the positive values of r_{Hopf} are physically meaningful. By letting ω increase from zero, we obtain on the parameter plane the multibranched curve of the Hopf bifurcation.

The starting point of the Hopf curve corresponds to $\omega = 0$; here, the linearized flow has two vanishing eigenvalues. The value of r for this codimension-2 bifurcation ("double zero" or a Takens-Bogdanov point) is

$$r_{\mathrm{TB}} = \frac{\tau_2 \alpha_3(\alpha_2 + 1)}{\tau_2\tau_3\alpha_3(\alpha_2 - 1) + \alpha_2(\alpha_3 + 1)\tau_3^2}, \tag{23}$$

and s must satisfy Eq. (20). On the parameter plane spanned by r and s, the curve of the Hopf bifurcation joins in this point the saddle-node curve. Yet another bifurcation curve starts in the Takens-Bogdanov point, the curve of a homoclinic bifurcation, at which the formation of the separatrix loop gives birth to the finite-amplitude periodic state. The latter bifurcation is a global event and can only be traced numerically. Numerical localization of the homoclinic bifurcation and of the tangent bifurcation in which finite-amplitude periodic solutions disappear is beyond the scope of our analysis, restricted to local bifurcations of steady states.

Remarkably, the "triple zero" (codimension-3 bifurcation when three eigenvalues vanish simultaneously), which gives rise to complicated nonlinear states including chaotic attractors, cannot occur in Eq. (18): irrespectively of the shape of the dependence $\gamma(P)$, triple zero is incompatible with conditions $\tau_i > 0$, $\alpha_i \geq 1$.

In the next subsections we briefly review a few particular cases.

C. Some limiting cases

The Markovian case $\alpha_2 = \alpha_3 = 1$ corresponds to exponentially distributed waiting times in states 2 and 3. Here, the characteristic equation reduces to the quadratic one

$$\tau_2\tau_3\lambda^2 + [\tau_2 + \tau_3 + (r - s)\tau_2\tau_3]\lambda + 1 - s\tau_2 + r(\tau_2 + \tau_3) = 0.$$

The corresponding mean-field equations (16) can be rewritten as two ordinary autonomous differential equations supplemented with the normalization condition. The Hopf bifurcation with onset of self-sustained oscillations occurs at

$$s = r + \frac{\tau_2 + \tau_3}{\tau_2\tau_3} \tag{24}$$

under the provision $r > \tau_2/\tau_3^2$. We mention that an investigation of unidirectional cyclic coupling has disclosed the existence of oscillations in the Markovian model [52,53]. Since the phase space is two dimensional, the set of possible attractors for collective dynamics is restricted to equilibria and periodic oscillations.

The opposite limit $\alpha_2, \alpha_3 \to \infty$ describes fixed waiting times in states 2 and 3 (see Fig. 6). The characteristic equation turns into

$$1 - \frac{s(1 - e^{-\lambda\tau_2}) - r(1 - e^{-\lambda(\tau_2 + \tau_3)})}{\lambda} = 0. \tag{25}$$

This transcendental equation has infinitely many roots, since the delay introduced by the fixed waiting times makes the evolution equations for two variables $P_2(t)$ and $P_3(t)$ infinite dimensional. The saddle-node bifurcation is invariably given by the condition (20). The multibranched curve of the Hopf bifurcation on the parameter plane of r and s is rendered in the parametric form

$$r = \omega \frac{\cos\omega\tau_2 - 1}{\sin\omega\tau_2 + \sin\omega\tau_3 - \sin\omega(\tau_2 + \tau_3)},$$

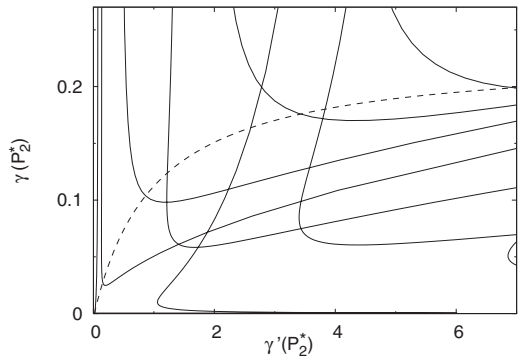

FIG. 7. Bifurcation curves for the case of fixed waiting times. $\tau_2=65$; $\tau_3=220$. Solid lines: Hopf bifurcations. Dashed line: saddle-node bifurcation. Intersection of dashed line with solid curves: fold-Hopf points. Intersections of solid lines: "double Hopf" points.

$$s = \omega \frac{\cos\,\omega(\tau_2+\tau_3)-1}{\sin\,\omega\tau_2+\sin\,\omega\tau_3-\sin\,\omega(\tau_2+\tau_3)},$$

where the frequency of the critical oscillations ω runs through all positive numbers (of course, again, only positive values of the rate r are meaningful). More involved dynamics, including homoclinic solutions, can be encountered near the codimension-2 points on the parameter plane, the unique Takens-Bogdanov point at

$$r_{\mathrm{tb}} = \frac{\tau_2}{\tau_3(\tau_2+\tau_3)},$$

and the family of fold-Hopf (or Gavrilov-Guckenheimer) points where the characteristic equation (25) possesses simultaneously two purely imaginary roots and a zero root. This event takes place for

$$r_{\mathrm{fh}} = \frac{\sin\,\omega\tau_2-\omega\tau_2}{\tau_2\,\sin\,\omega(\tau_2+\tau_3)-(\tau_2+\tau_3)\sin\,\omega\tau_2},$$

where the frequency of critical oscillations ω solves the transcendental equation

$$\omega[\tau_3-(\tau_2+\tau_3)\cos\,\omega\tau_2+\tau_2\,\cos\,\omega(\tau_2+\tau_3)] = \sin\,\omega\tau_2+\sin\,\omega\tau_2-\sin\,\omega(\tau_2+\tau_3).$$

For example, for $\tau_2=65$ and $\tau_3=220$ the fold-Hopf bifurcations occur at $r=0.028\,964\,3$ (with $\omega=0.1055$), $r=0.103\,835$ ($\omega=0.204\,29$), $r=0.125\,980$ ($\omega=0.137\,57$),…, whereas the corresponding value of s is in each case given by (20).

A typical bifurcation diagram on the plane spanned by $\gamma'(P_2^*)=s[1+r(\tau_2+\tau_3)]$ and $\gamma(P_2^*)=r$ is presented in Fig. 7. The dashed line, which corresponds to the saddle-node bifurcation, repeatedly intersects the branches of the Hopf bifurcation curves; each of these intersections delivers a fold-Hopf point. Furthermore, different branches of the Hopf curve intersect each other. At each intersection, the characteristic equation (25) possesses two pairs of imaginary eigenvalues. According to the general bifurcation theory, in the neighborhood of such codimension-2 "double Hopf" points the system can demonstrate complicated dynamics, including quasiperiodic and chaotic states.

Between the Markovian limit and the limit of fixed waiting times, α_2 and α_3 assume real values. In the cases when those values are integers (Erlang density), the convolution of states 2 and 3 can be reshaped as a finite set of ordinary differential equations. This possibility relies on the known property of the Γ-density function with integer α_i. The convolution of states 2 and 3, whose probabilities P_2 and P_3 follow non-Markovian dynamics, is mapped to α_2 substates $(2,i)$ and α_3 substates $(3,j)$, respectively. The corresponding probabilities $P_{2,i}$ and $P_{3,j}$ obey the ordinary differential equations (ODEs)

$$\frac{d}{dt}P_1(t) = -\gamma\left(\sum_{i=1}^{\alpha_2} P_{2,i}(t)\right)P_1(t)+\frac{\alpha_3}{\tau_3}P_{3,\alpha_3}(t),$$

$$\frac{d}{dt}P_{2,1}(t) = \gamma\left(\sum_{i=1}^{\alpha_2} P_{2,i}(t)\right)P_1(t)-\frac{\alpha_2}{\tau_2}P_{2,1}(t),$$

$$\frac{d}{dt}P_{2,i}(t) = \frac{\alpha_2}{\tau_2}[P_{2,i-1}(t)-P_{2,i}(t)],\quad i=2,\ldots,\alpha_2,$$

$$\frac{d}{dt}P_{3,i}(t) = \frac{\alpha_3}{\tau_3}[P_{3,j-1}(t)-P_{3,j}(t)],\quad j=2,\ldots,\alpha_3,$$

$$\frac{d}{dt}P_{3,1}(t) = \frac{\alpha_2}{\tau_2}P_{2,\alpha_2}(t)-\frac{\alpha_3}{\tau_3}P_{3,1}(t). \tag{26}$$

For such finite-dimensional systems, the stability of steady states can be determined, e.g., by applying the Routh-Hurwitz criterion to linearization matrices at the fixed points. Further, a weakly nonlinear analysis decides whether the Hopf bifurcation is subcritical or supercritical (see also [54]). For $\max(\alpha_i)>1$, the dimension $\alpha_2+\alpha_3$ of the phase space allows, in principle, for more complicated dynamics than periodic processes.

D. Excitatory coupling is necessary for oscillations

Below, we call the coupling excitatory if the rate γ increases with growing population in state 2. If transitions $1\to 2$ become less probable with increasing P_2, the coupling is called inhibitory. We show that inhibitory coupling does not destabilize the stationary solution, and spontaneous oscillations do not occur. To this end we rewrite the characteristic Eq. (18) as

$$1-s\hat{z}_2(\lambda)+r\hat{z}_{23}(\lambda)=0. \tag{27}$$

The $\hat{z}_k$ denote Laplace transforms of the survival probabilities,

$$\hat{z}_k(\lambda)=\int_0^\infty d\tau\,\exp(-\lambda\tau)z_k(\tau), \tag{28}$$

and z_{23} stands for the probability to survive longer than τ in states 2 and 3 together:

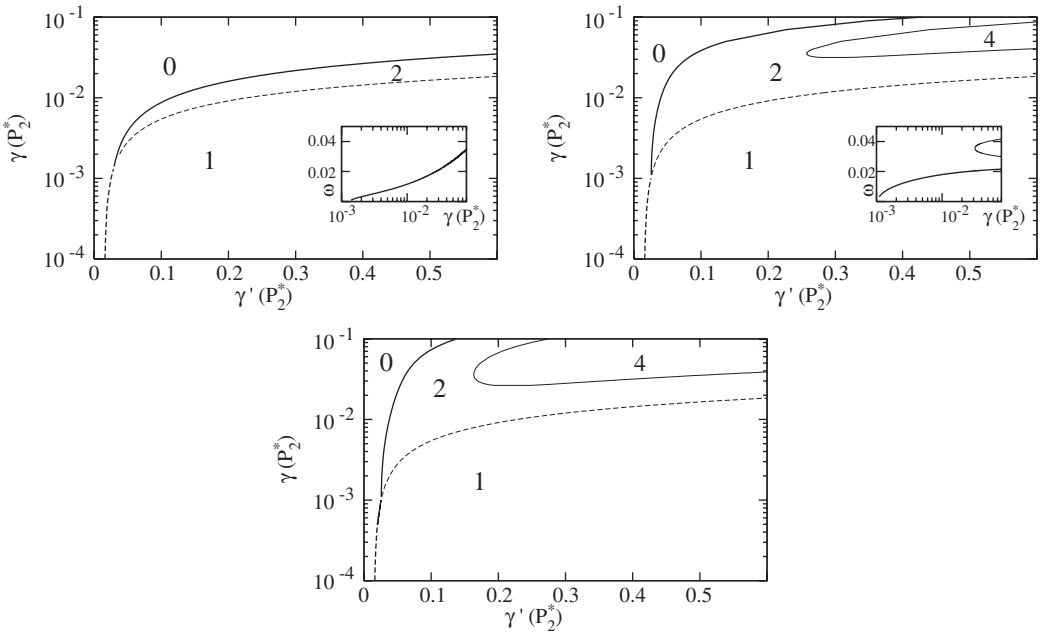

FIG. 8. Number of roots of Eq. (29) with positive real part as a function of the stationary rate $\gamma(P_2^*)$ and its derivative $\gamma'(P_2^*)$ for $\tau_2=65$, $\tau_3=220$, and different values of $n=\alpha_2=\alpha_3$. From top to bottom: $n=20$, 100, 500. Solid lines: Hopf bifurcations. Evolution of frequency along the bifurcation line is plotted in the inset. Dashed lines: vanishing real root of the characteristic equation.

$$z_{23}(\tau) = 1 - \int_0^\tau d\tau' (w_2 \circ w_3)(\tau').$$

Equation (27) has no solutions λ with positive real part. To demonstrate this we assume that λ with $\mathrm{Re}\,\lambda > 0$ is a solution. As the survival probabilities $z_k(\tau)$ are positive and monotonically decreasing functions of τ, we deduce that the imaginary part of their Laplace transform $\hat{z}_k(\lambda)$, Eq. (28) is positive if $\mathrm{Im}\,\lambda > 0$; that it is negative if $\mathrm{Im}\,\lambda < 0$ and it equals 0 if $\mathrm{Im}\,\lambda = 0$. An inhibitory coupling $\gamma'(P_2) < 0$ implies $s < 0$ and thus both coefficients of the imaginary parts of the Laplace transforms are positive. Consequently, the imaginary part of Eq. (27) has only a solution if $\mathrm{Im}\, z_2(\lambda) = \mathrm{Im}\, \hat{z}_{23}(\lambda) = 0$—i.e., if $\mathrm{Im}\,\lambda = 0$. However, in this case $\mathrm{Re}\, z_2(\lambda) > 0$ and $\mathrm{Re}\, \hat{z}_{23}(\lambda) > 0$ and thus the real part of Eq. (27) has no solution. Thus we can exclude solutions of the characteristic equation with positive real part; i.e., the stationary solution always remains stable.

E. Transition scenario to synchronized behavior

To investigate whether Eq. (25) has solutions with positive real part, we transform it to

$$\left(1 + \frac{\tau_2\lambda}{\alpha_2}\right)^{\alpha_2}\left(1 + \frac{\tau_3\lambda}{\alpha_3}\right)^{\alpha_3}\left(1 - \frac{s}{\lambda} + \frac{r}{\lambda}\right) + \frac{s}{\lambda}\left(1 + \frac{\tau_3\lambda}{\alpha_3}\right)^{\alpha_3} - \frac{r}{\lambda} = 0. \quad (29)$$

When both α_2 and α_3 are integers, this is a polynomial equation in λ (the terms proportional to $1/\lambda$ cancel). Equations of this type generally occur in the stability analysis of delay differential equations [55].

We calculated the number of roots with positive real part with the help of the Routh-Hurwitz criterion [56]. Results were utilized for a numerical search of bifurcations. For large integer values of α_i the conventional machine precision turns out to be insufficient, and we had to resort to the arbitrary precision arithmetic of Mathematica, which automatically keeps track of the errors.

We consider the influence of the variances α_i of the waiting times in states 2 and 3. In Fig. 8 the number of roots of the characteristic equation with positive real part is shown as function of the rate $\gamma(P_2^*)$ and its derivative $\gamma'(P_2^*)$. This number gives the dimension of the unstable manifold of the considered fixed point in the enlarged state space.

To mimic the waiting times of the FHN system (cf. Fig. 2) we take for the mean waiting times in states 2 and 3 the values $\tau_2=65$ and $\tau_3=220$. For the variances, three integer values $n=\alpha_2=\alpha_3$ are taken: $n=20$, $n=100$, and $n=500$. Recall that the variance of the waiting times in the excited and refractory states decreases with the growth of n, in accordance with Eq. (4).

We observe that for large stationary rate $\gamma(P_2^*)$, the increase of $\gamma'(P_2^*)$ destabilizes the stationary solution via a Hopf bifurcation: Two complex conjugated eigenvalues acquire positive real parts. The location of this bifurcation strongly depends on $\alpha_2=\alpha_3=n$. The higher n is, the larger the region of instability. This implies that a sharply peaked excited and refractory time supports coherent oscillations and thus the synchronization among the units. The frequency at the Hopf bifurcation is shown in the insets of Fig. 8. Noteworthy, the frequency jumps if a loop is created along the bifurcation line (cf. Fig. 9).

Linearized numerical analysis does not allow to decide whether the Hopf bifurcation is supercritical or subcritical.

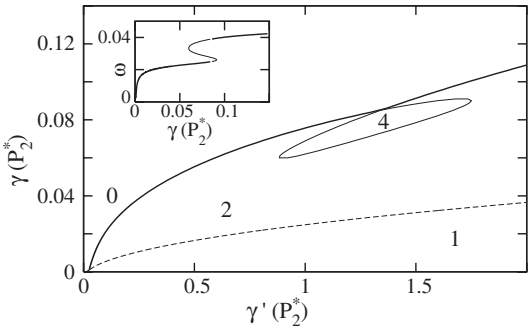

FIG. 9. Number of solutions of Eq. (29) with positive real part as a function of the stationary rate $\gamma(P_2^*)$ and its derivative $\gamma'(P_2^*)$ for $n=20$ as in Fig. 8. The loop on the curve of the Hopf bifurcation invokes a jump in the frequency of the oscillations.

For this purpose, the higher-order terms in Eq. (8) have to be taken into account. The center manifold theorem [57] for functional differential equations holds in general; in our case, we found it more convenient to work within enlarged phase space [see Eqs. (26)]. Explicit algebraic computation of the branching coefficient has allowed us to distinguish between supercritical and subcritical Hopf bifurcation.

IV. ARRHENIUS-TYPE EXCITATORY COUPLING

As an illustration, we consider the behavior of coupled units for an Arrhenius-type excitation rate. We assume that the effective potential barrier, which a system has to surpass in order to be excited from the rest state, depends on the fraction of neighbors in state 2. This leads to the rate as a function of P_2:

$$\gamma(P_2) = \gamma_0 \exp\left(-\frac{\Delta U(P_2)}{D}\right). \tag{30}$$

An affine relation between the potential barrier and coupling parameter is considered. For simplicity we assume the linear dependence

$$\Delta U(P_2) = \Delta U_0(1 - \sigma P_2),$$

with ΔU_0 being the barrier of an individual unit and coupling strength σ.

The stationary rate $\gamma(P_2^*)$ as a function of coupling strength σ and the noise intensity D can be expressed as [see Eq. (17)]

$$\gamma(P_2^*) = \gamma_0 e^{\Delta U_0(1-\sigma P_2^*)/D} = \frac{P_2^*}{\tau_2 - P_2^*(\tau_2 + \tau_3)}.$$

Similarly, the derivative of the rate in the stationary state $\gamma'(P_2^*)$ is reshaped as

$$\gamma'(P_2^*) = \frac{\gamma_0 \sigma \Delta U_0}{D} e^{\Delta U_0(1-\sigma P_2^*)/D} = \frac{\sigma \Delta U_0}{D} \frac{P_2^*}{\tau_2 - P_2^*(\tau_2 + \tau_3)}.$$

In both expressions P_2^* is the solution of the equation

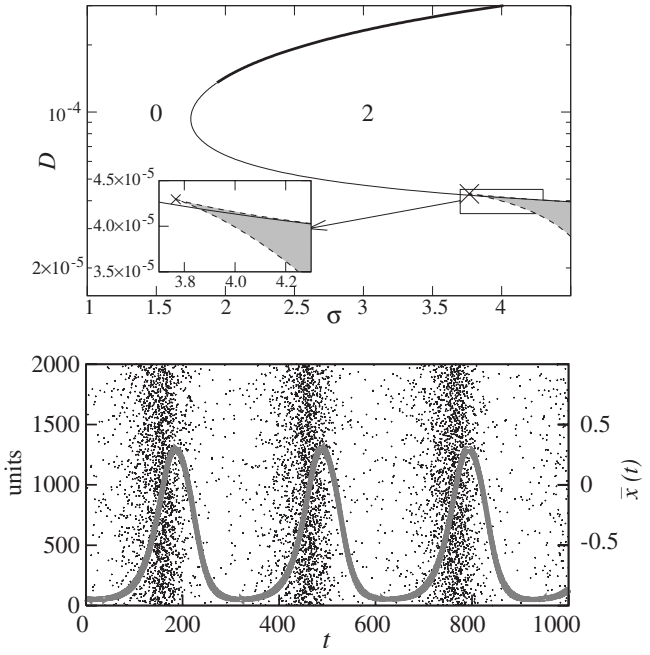

FIG. 10. Top: bifurcation diagram for the Arrhenius type-rate: Eq. (30) with $\Delta U_0=0.0002$, $\gamma_0=0.05$, and other parameter values as in Fig. 8. For sufficiently high noise intensity D, an increase of the coupling strength σ leads to the Hopf bifurcation (solid line) and thus to oscillating behavior. The Hopf bifurcation is supercritical along the thick segment of the solid line and subcritical along the thin segment. Dashed lines: saddle-node bifurcation. The cusp point, as given by condition (21), is indicated by the cross. There are three steady solutions in the shaded region and the single steady solution outside it. Bottom: numerical simulation of the 100 000 coupled three-state models (2000 are shown). Black dots indicates moments where transitions from state 1 to state 2 take place. The gray solid line shows the mean output $\bar{x}(t)=P_2(t)-[P_1(t)+P_3(t)]=2P_2(t)-1$. Parameters as in the upper curve and $D=0.0002$ and $\sigma=3$.

$$P_2^* = \frac{\tau_2}{\tau_2 + \tau_3 + \frac{1}{\gamma_0}\exp\left(\frac{\Delta U_0(1-\sigma P_2^*)}{D}\right)}. \tag{31}$$

Since Eq. (31) can have more than one solution, there can be several pairs $(\gamma(P_2^*), \gamma'(P_2^*))$ which correspond to the given pair (σ, D). Conversely, a pair of values $(\gamma(P_2^*), \gamma'(P_2^*))$ uniquely defines the pair(σ, D) by

$$\sigma = \frac{\gamma'(P_2^*)T}{\gamma'(P_2^*)\tau_2 + \gamma(P_2^*)T \ln\left(\frac{\gamma_0}{\gamma(P_2^*)}\right)},$$

$$D = \frac{\sigma \Delta U_0 \gamma(P_2^*)}{\gamma'(P_2^*)} = \frac{T \Delta U_0 \gamma(P_2^*)}{\gamma'(P_2^*)\tau_2 + \gamma(P_2^*)T \ln\left(\frac{\gamma_0}{\gamma(P_2^*)}\right)}, \tag{32}$$

with T being the mean duration of a cycle: $T=\tau_2+\tau_3+1/\gamma(P_2^*)$.

As a rough estimate of the FHN system with parameters from Fig. 2, we substitute $\Delta U=0.0002$ and $\gamma_0=0.05$ in Eq. (30). By using the relations (32) we can now map the bifur-

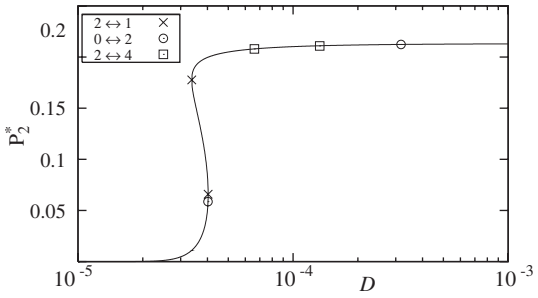

FIG. 11. Stationary solution P_2^* as a function of noise strength for $\sigma=4.3$. Marks (cross, circles, squares): changes in the number of eigenvalues with positive real part.

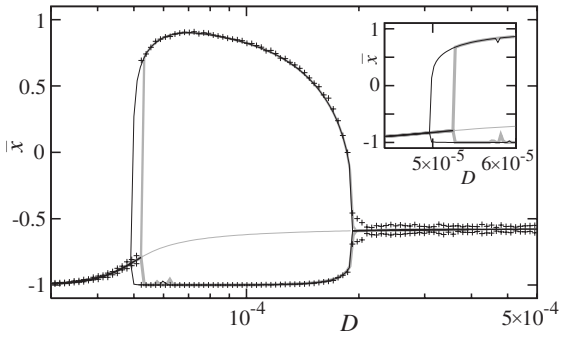

FIG. 12. Arrhenius-type excitation rate (30) with $\sigma=2.5$; other parameters as in Fig. 10. Stationary mean output and extrema of the time-dependent mean output $\bar{x}(t)=P_2(t)-[P_1(t)+P_3(t)]=2P_2(t)-1$ for oscillatory solutions. Symbols: simulations of an ensemble of 10^4 coupled three-state units. Thick gray and thin black lines: simulation of the ODE (26). Thin gray and thick black lines: stationary solution (respectively, stable and unstable) of Eq. (31). Inset: hysteresis near the subcritical Hopf bifurcation.

cation diagrams from the space spanned by $\gamma(P_2^*)$ and $\gamma'(P_2^*)$ (cf. Figs. 8 and 9) into the parameter space of σ and D. The result is presented in Fig. 10.

According to the diagram, oscillatory behavior is found if the coupling σ is sufficiently strong. An increase of the noise intensity D leads from nonoscillatory to oscillatory and back to nonoscillatory dynamics. The details of this process with a fixed value of σ are shown in Fig. 11. If the noise is rather weak, the steady state is unique and stable. An increase of the noise amplitude generates by means of the saddle-node bifurcation two additional unstable fixed points. The stable stationary solution is destabilized in the course of the subcritical Hopf bifurcation. On increasing the noise strength further, this unstable stationary state merges with another saddle point and vanishes in the saddle-node bifurcation. Finally, the remaining stationary solution regains stability via the Hopf bifurcation, which in this case is supercritical.

At a certain noise level the amplitude of the limit cycle attains a maximum, indicating coherence resonance (see Fig. 12). Finally the limit cycle vanishes and the stationary solution becomes stable again.

Finally, we compare the behavior of the ensemble of globally coupled discrete three-state models to a system of globally coupled FHN units. As in the discrete model, the coupling works via the mean activator value of the ensemble $\bar{x}=\frac{1}{N}\Sigma_{i=1}^{N}x_i$:

$$\dot{x}_i = x_i - x_i^3 - y_i + c\bar{x} + \sqrt{2D}\xi_i(t),$$

$$\dot{y}_i = \varepsilon(x_i + a_0 - a_1 y_i), \tag{33}$$

where the coupling strength is denoted by c and $\xi_i(t)$ is local Gaussian white noise with $\langle \xi_i(t)\xi_j(t+\tau)\rangle = \delta_{i,j}\delta(\tau)$. The stationary radius of the oscillations of the mean field as a function of noise intensity D and coupling strength c is shown in Fig. 13. Qualitative agreement with the results presented in Figs. 10 and 12 is well visible. The quantitative deviations for larger noise intensity D arise from the noise dependence of the waiting time densities in the three states. Both the Arrhenius-like dependence [see Eq. (30)] of the rate γ as well as the constancy of width of the waiting time densities in the excited and refractory states [see Eq. (5a) and (5b)] can hardly be expected to hold for larger noise.

V. CONCLUSIONS

To conclude, we considered ensembles of discrete stochastic units which constitute a generic model of coupled

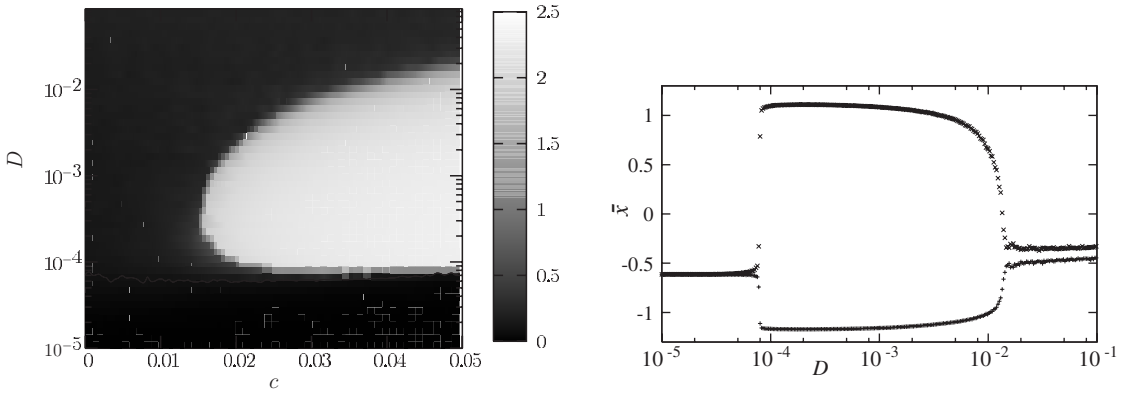

FIG. 13. Dynamical characteristics for 2×10^3 globally coupled FHN systems governed by Eq. (33). Top: oscillation amplitude of the mean output $\bar{x}(t)$ as a function of coupling strength c and noise intensity D. Bottom: maximal and minimal values of the mean output $\bar{x}(t)$ versus noise intensity for $c=0.04$. Other parameters as in Fig. 2.

excitable systems. When coupled, the ensemble reproduces the well-known behavior of coherent oscillations [33,36]. Due to its relative simplicity, the dynamics is described by a set of two integral equations for the mean fields and the normalization condition. Bifurcation analysis reveals destabilization of the steady state and the onset of oscillations under a variation of the system parameters, such as noise intensity and coupling strength. Numerical simulations indicate that these mechanisms remain valid also for sufficiently large finite systems.

We acknowledge support by DFG Grant No.Sfb-555. We are grateful to B. Naundorf (Göttingen) and E. Schöll (TU Berlin) for stimulating discussions.

[1] N. G. van Kampen, *Stochastic Processes in Physics and Chemistry* (North-Holland, Amsterdam, 1992).
[2] H. C. Tuckwell, *Introduction to Theoretical Neurobiology* (Cambridge University Press, Cambridge, England, 1988), Vol. 2.
[3] D. S. Fisher and D. A. Huse, Phys. Rev. B **38**, 373 (1988).
[4] R. Sànchez, D. E. Newman, and B. A. Carreras, Phys. Rev. Lett. **88**, 068302 (2002).
[5] H. Weissman, G. H. Weiss, and S. Havlin, J. Stat. Phys. **57**, 301 (1989).
[6] S. Fedotov and Y. Okuda, Phys. Rev. E **66**, 021113 (2002).
[7] M. F. Shlesinger, J. Stat. Phys. **10**, 421 (1974).
[8] Th. M. Nieuwenhuizen and M. H. Ernst, J. Stat. Phys. **41**, 773 (1985).
[9] C. Van den Broeck, Phys. Rev. Lett. **62**, 1421 (1989).
[10] R. Cox, *Renewal Theory* (Methuen, London, 1965).
[11] T. Prager, B. Naundorf, and L. Schimansky-Geier, Physica A **325**, 176 (2003).
[12] B. Lindner, J. García-Ojalvo, A. Neiman, and L. Schimansky-Geier, Phys. Rep. **392**, 321 (2004).
[13] B. S. Gutkin and G. B. Ermentrout, Neural Comput. **10**, 1047 (1998).
[14] M. Falcke, Adv. Phys. **53**, 255 (2004).
[15] N. Wiener and A. Rosenbluth, Arch. Inst. Cardiol. Mex. **16**, 205 (1946).
[16] H. Hempel, L. Schimansky-Geier, and J. García-Ojalvo, Phys. Rev. Lett. **82**, 3713 (1999).
[17] A. Neiman, L. Schimansky-Geier, A. Cornell-Bell, and F. Moss, Phys. Rev. Lett. **83**, 4896 (1999).
[18] Changsong Zhou, Jürgen Kurths, and Bambi Hu, Phys. Rev. Lett. **87**, 098101 (2001).
[19] H. Busch and F. Kaiser, Phys. Rev. E **67**, 041105 (2003).
[20] H. Haken, *Advanced Synergetics* (Springer, Berlin, 1983).
[21] A. T. Winfree, J. Theor. Biol. **16**, 15 (1967); **28**, 327 (1970).
[22] Y. Kuramoto, in *Proceedings of the International Symposium on Mathematical Problems in Theoretical Physics*, edited by H. Arakai (Springer, New York, 1975), Vol. 39.
[23] S. H. Strogatz, Physica D **143**, 1 (2000).
[24] V. S. Anishchenko, V. V. Astakhov, A. B. Neiman, T. E. Vadivasova, and L. Schimansky-Geier, *Nonlinear Dynamics of Chaotic and Stochastic Systems* (Springer, Berlin, 2002).
[25] A. Pikovsky, M. Rosenblum, and J. Kurths, *Synchronization* (Cambridge Univversity Press, Cambridge, England, 2001).
[26] Z. Néda, E. Ravasz, Y. Brechet, T. Vicsek, and A. L. Barabási, Nature (London) **403**, 849 (2000).
[27] A. K. Engel, P. Fries, and W. Singer, Nat. Rev. Neurosci. **2**, 704 (2001).
[28] P. A. Tass, *Phase Resetting in Medicine and Biology-Stochastic Modelling and Data Analysis* (Springer, Berlin, 1999).
[29] C. Fohlmeister, R. Ritz, W. Gerstner, and J. L. van Hemmen, Neural Comput. **7**, 905 (1995).
[30] Y. Kuramoto, *Chemical Oscillations, Waves and Turbulence* (Springer, New York, 1984).
[31] A. S. Mikhailov, *Foundation of Synergetics* (Springer, Berlin, 1992).
[32] A. Ganopolski and S. Rahmstorf, Phys. Rev. Lett. **88**, 038501 (2002).
[33] H. Sakaguchi, S. Shinomoto, and Y. Kuramoto, Prog. Theor. Phys. **79**, 600 (1988).
[34] A. Nikitin, Z. Néda, and T. Vicsek, Phys. Rev. Lett. **87**, 024101 (2001).
[35] B. Hu and C. S. Zhou, Phys. Rev. E **61**, R1001 (2000).
[36] M. A. Zaks, A. B. Neiman, S. Feistel, and L. Schimansky-Geier, Phys. Rev. E **68**, 066206 (2003).
[37] W. Ebeling, H. Herzel, W. Richert, and L. Schimansky-Geier, Z. Angew. Math. Mech. **66**, 141 (1986).
[38] H. Treutlein and K. Schulten, Ber. Bunsenges. Phys. Chem **89**, 710 (1985).
[39] D. Sigeti and W. Horsthemke, J. Stat. Phys. **54**, 1217 (1989).
[40] Hu Gang , T. Ditzinger, C. Z. Ning, and H. Haken, Phys. Rev. Lett. **71**, 807 (1993).
[41] A. S. Pikovsky and J. Kurths, Phys. Rev. Lett. **78**, 775 (1997).
[42] V. Nollau, *Semi-Markovsche Prozesse* (Akademie, Berlin, 1980).
[43] J. Sneyd and J. P. Keener, *Mathematical Physiology* (Springer, Berlin, 1999).
[44] P. Talkner, Physica A **325**, 124 (2003).
[45] N. Brunel, V. Hakim, and M. J. E. Richardson, Phys. Rev. E **67**, 051916 (2003).
[46] M. Schindler, P. Talkner, and P. Hänggi, Phys. Rev. Lett. **93**, 048102 (2004).
[47] T. Verechtchaguina, I. M. Sokolov, and L. Schimansky-Geier, Phys. Rev. E **73**, 031108 (2006).
[48] R. Thul and M. Falcke (unpublished).
[49] R. L. Stratonovich, *Topics in the Theory of Random Noise I* (Gordon and Breach, New York, 1962).
[50] Notably, without summation these equations do not hold, e.g., in general $p(\ldots,\sigma_{j-1},2,\sigma_{j+1},\ldots,t) \neq \int_0^\infty d\tau\, \gamma(n_2/N) p(\ldots,\sigma_{j-1},1,\sigma_{j+1},\ldots,t-\tau) z_2(\tau)$ because in the time interval between the value $t-\tau$ when the unit j leaves state 1 and the value t at which we evaluate the probability of unit j to be in state 2, other units may arbitrarily change their states.
[51] Variation of r and p corresponds to the motion in the parameter space. Note, however, that each pair (r,s) is defined through only one of possibly multiple coexisting steady states; there-

fore, several different points on the plane r,s may correspond to the very same set of "genuine" external parameters.

[52] K. Wood, C. Van den Broeck, R. Kawai, and K. Lindenberg, Phys. Rev. Lett. **96**, 145701 (2006).

[53] K. Wood, C. Van den Broeck, R. Kawai, and K. Lindenberg, Phys. Rev. E **74**, 031113 (2006).

[54] T. Prager, Ph.D. thesis, Humboldt-University at Berlin, 2006.

[55] R. Bellman, *Differential-Difference Equations* (Academic Press, New York, 1963).

[56] F. R. Gantmacher, *Applications of the Theory of Matrices* (Wiley, New York, 1959), p. 230.

[57] J. K. Hale and S. M. V. Lunel, *Introduction to Functional Differential Equations*, Vol. 99 of Applied Mathematical Sciences (Springer-Verlag, New York, 1993.)